Journal of Magnetics 14(2), 75-79 (2009)

Synthesis of Metal and Ceramic Magnetic Nanoparticles by Levitational Gas Condensation (LGC)

Y. R. Uhm*, H. M. Lee, G. J. Lee, and C. K. Rhee

Nuclear Materials Research Division, Korea Atomic Energy Research Institute, Daejeon 305-353, Korea

(Received 15 January 2009, Received in final form 2 April 2009, Accepted 2 April 2009)

Nickel (Ni) and ferrite (Fe_3O_4, $NiFe_2O_4$) nanoparticles were synthesized by LGC using both wire feeding (WF) and micron powder feeding (MPF) systems. Phase evolution and magnetic properties were then investigated. The Ni nanopowder included magnetic-ordered phases. The LGC synthesis yielded spherical particles with large coercivity while the abnormal initial magnetization curve for Ni indicated a non-collinear magnetic structure between the core and surface layer of the particles. Since the XRD pattern cannot actually distinguish between magnetite (Fe_3O_4) and maghemite (γ-Fe_2O_3) as they have a spinel type structure, the phase of the iron oxide in the samples was unveiled by Mössbauer spectroscopy. The synthesized Ni-ferrite consisted of single domain particles, including an unusual ionic state. The synthesized nanopowder bore an active surface due to the defects that affected abnormal magnetic properties.

Keywords : nanopowder, levitational gas condensation (LGC)

1. Introduction

The development of new methods for nanopowder synthesis such as magnetron sputtering, melt spinning, and mechanical alloying, opens up new possibilities for non-equilibrium phases and nanocrystalline materials with new and unusual physical properties applicable to p-type semiconductors, catalysts, and drug delivery systems [1-2]. Among the various established preparation methods for nanopowders, mechanical alloying, micro-emulsion, sol-gel, and hydrothermal processes [3-5], simplicity, cost effectiveness, and environmental soundness are key. The levitational gas condensation (LGC) method is just such an approach [6]. In previous studies, the complicated levitation and evaporation mechanism for fabrication were explained thoroughly [6]. It has also been reported that a nanopowder synthesized by gas phase methods showed unusual magnetic properties due to a surface effects [7, 8]. However, it is impossible to synthesize several complicated metal doping materials such as ferrites, perovskite, garnet, metal-doped ZnO, Ti-Ni, and Al-Ni-Co, because the supply of the parent materials into the levitated drop in the induction coil was a wire feeding system. Nevertheless, the newly modified micron powder feeding system (MPF) overcame this doping problem of the LGC system [9].

In this study, several magnetic particles were synthesized by a simple, one-step levitational gas condensation (LGC) method using an MPF system, and the magnetic properties, including ionic states of the iron, were investigated by Mössbauer spectroscopy.

2. Experimental Technique

2.1. Synthesis of Magnetic Metal Nanoparticles (Ni)

A schematic illustration of the equipment for preparing the nanoparticles *via* LGC is shown in Ref. [6]. A suspended melt drop blown by inert gas (Ar) is heated to 2000°C by a high-frequency induction generator. The metallic atoms, evaporated from the overheated surface, were condensed by a cold inert gas and collected from the filter. To stabilize the powder surface, the powders were passivated with thin oxide layers. The apparatus consisted of a high-frequency induction generator of 6 kW, a levitation and evaporation chamber, and an oxygen concentration control unit. The wire feeding velocities for nickel (V_{Ni}) were 50 mm/min. The Ar pressure in the chamber was 18 kPa.

*Corresponding author: Tel: +82-42-868-4835
Fax: +82-42-868-4847, e-mail: uyrang@kaeri.re.kr

2.2. Synthesis of Ferrite Nanoparticles (Fe_3O_4, $NiFe_2O_4$)

High purity Fe_2O_3 powders were synthesized by a LGC method. The apparatus consisted of a high frequency induction generator of 5 kW, a levitation and evaporation chamber, and an oxygen concentration control unit. The wire feeding velocity (V_{Fe}) and mixed Ar and O_2 gas pressures in the chamber was 50 mm/min and 18 kPa, respectively.

The $NiFe_2O_4$ powders were synthesized by the LGC method using a micron powder feeding (MPF) system [9]. The apparatus consisted of a high-frequency induction generator of 6 kW. The starting materials were mixed micron powders of Ni and Fe at a size range of 100 to 500 μm. The amount of micron powder fed into the liquid droplet of the seed was controlled at 80 mg/min. The mixed Ar and O_2 gas pressures in the chamber were 18 kPa.

2.3. Characterization of Magnetic Nanoparticles

The as-prepared samples were characterized by XRD, vibrating sample magnetometry (VSM), and Mössbauer spectroscopy. Magnetization data were taken using a magnetometer, Lake Shore. Inc (Westerville, Ohio, USA). A Mössbauer spectrometer of the electromechanical type was used in the constant-acceleration mode [10].

3. Results and Discussion

3.1. Magnetic Metal Nanoparticles (Ni, Fe)

The nanocrystalline Ni synthesized by LGC using the wire feeding system was confirmed by its XRD pattern, Fig. 1. The XRD results show the lattice parameters and position of the main peaks of the Ni powders. A small amount of the NiO phase was found in the XRD patterns and the TEM images, resulting from a passivated layer on the powder surface.

The microstructure and phase composition of the Ni powders were studied with transmission electron microscopy (TEM). The particle consisted of a single domain. Powders with single domains were synthesized by a special gas phase method, though the average particle size was over 100 nm [7, 8]. Thin oxide layers on the powders formed a continuous coating at a thickness of 2.0-3.0 nm. Nanocrystalline Ni particles synthesized using the wire feeding (WF) system showed a spherical shape, Fig. 2. The TEM image showed that nanocrystalline Ni powders consisted of particles ranging from 15 to 40 nm.

The magnetic properties of the nanopowders were affected by the size effect resulting from the anisotropy field and magnetic domain effect on the particles [11]. The powders synthesized by LGC, showing low saturation

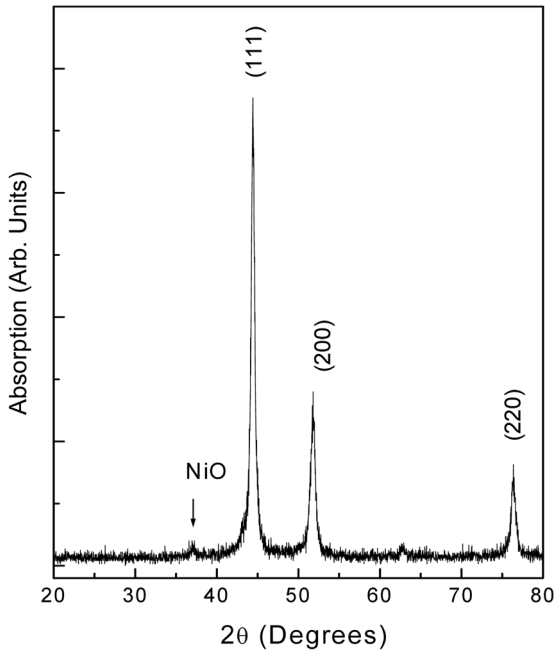

Fig. 1. X-ray diffraction (XRD) patterns using Cu-Kα for the Ni synthesized by LGC.

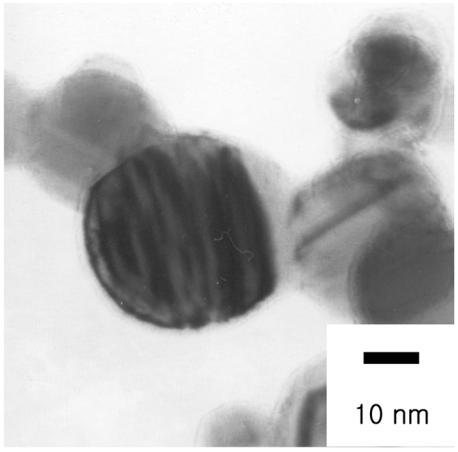

Fig. 2. TEM observation results show Ni synthesized using WF.

magnetization for the Ni, were probably due to the spin-coating effect and oxide phase on the surface [12]. The saturation magnetization was $M_S = 42$ emu/g. In Fig. 3, the hysteresis loop of the Ni in the low fields is shown. The slightly shifted hysteresis loop for the Ni sample can be explained by an exchange bias between the ferromagnetic core of the Ni and the antiferromagnetic surface of the NiO [9]; the hysteresis loop of the Ni in the low fields is shown. The symbol of the arrow indicates that the magnetization curve is placed out of the range of the hysteresis loop. The initial magnetization curve is not explained by size effect. More detailed analysis of the

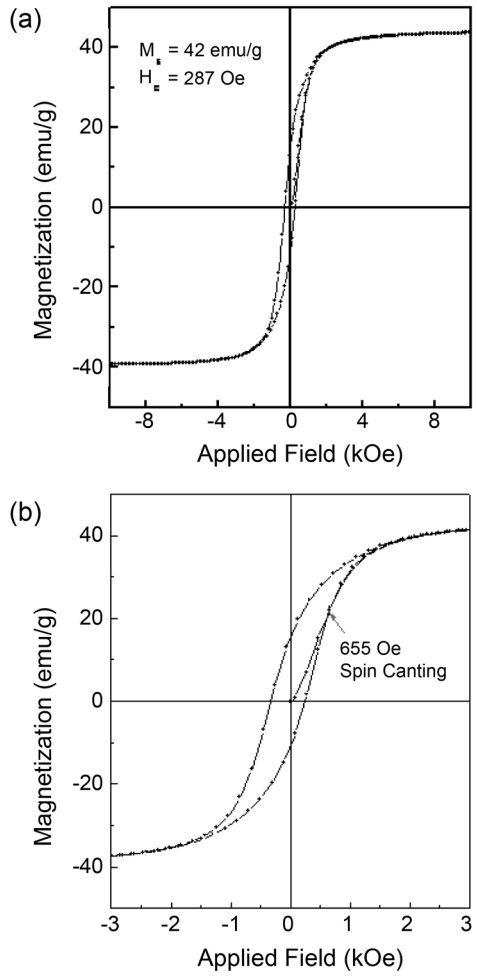

Fig. 3. Hysteresis loops for Ni (a) within an applied field of 10 kOe and (b) within an applied field of 3 kOe.

hysteresis properties of the Ni sample confirmed the non-collinear magnetic structure. The virgin magnetization curve slightly spilt over the limited hysteresis loop at 655 Oe, Fig. 3(b). It is assumed that this effect is enhanced when particle size reduced, which also increases the defects and the different magnetic structures on the surface of the particles [11]. The nature of this irreversibility in high magnetic fields allows for the description of a physical model [11, 12]. This irreversibility can be explained by spin-glass or spin-canting behavior.

3.2. Ferrite Nanoparticles (Fe_3O_4 and $NiFe_2O_4$)

A liquid droplet, levitated by the magnetic force acting against the gravitational force due to the coupled induction coils, is heated to 2000°C, causing the metallic atoms to evaporate from the overheated liquid droplet surface, condense by a cold inert gas, and collect into a filter. At the same time, the molecular O_2 introduced into the chamber is converted to atomic O with high activity under high

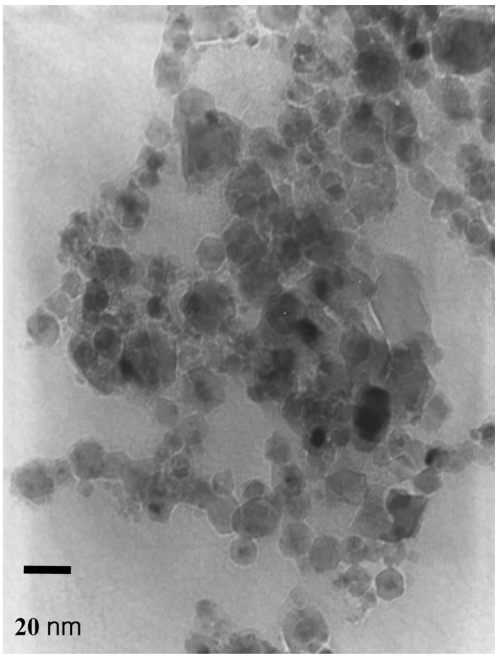

Fig. 4. TEM observation results showing the Fe_3O_4 under an O_2 flow rate of $0.15 \leq V_{O_2}$ (L/min) ≤ 0.2, synthesized by LGC.

temperature. The highly active O atoms can then diffuse into Fe clusters and react with the Fe atoms [6]. The α-Fe phase was observed at and below a $V_{O_2} = 0.05$ (L/min) oxygen flow rate. At and above a 0.2 (L/min) O_2 flow rate, levitation was not possible. The γ-Fe_2O_3 and α-Fe phase were observed at and below a $V_{O_2} = 0.15$ (L/min) oxygen flow rate. At and above 0.15 (L/min), nanocrystalline Fe_3O_4 phases were synthesized. Fig. 4 shows the TEM images, indicating that the nanocrystalline Fe_3O_4 powders were spherical with sizes ranging from 14 to 30 nm.

Since the XRD pattern cannot actually distinguish between magnetite (Fe_3O_4) and maghemite (γ-Fe_2O_3), given their spinel-type structures, the phase of iron oxide in the samples was unveiled by the Mössbauer spectrum as shown in Fig. 5. The structure of the magnetite (Fe_3O_4) consisted of 2 sub-structures of the octahedral (O_h) and tetrahedral (T_d) sites, including Fe^{2+} and Fe^{3+}, respectively [13]. The isomer shifts and the magnetic hyperfine interaction field of the Mössbauer spectrum and information on the valence state of iron. The Mössbauer spectrum at room temperature in Fig. 5(a) consisted of 2 sets of sextet Lorentzian lines. Two superimposed sextets corresponded to α-Fe and Fe^{3+} of the γ-Fe_2O_3, respectively [14]. The parameters of the Mössbauer spectrum were consistent with the hyperfine values reported for γ-Fe_2O_3 by R. M. Cornell *et al.* [15] A detailed analysis yielded that the respective amounts of α-Fe and γ-Fe_2O_3 were 7

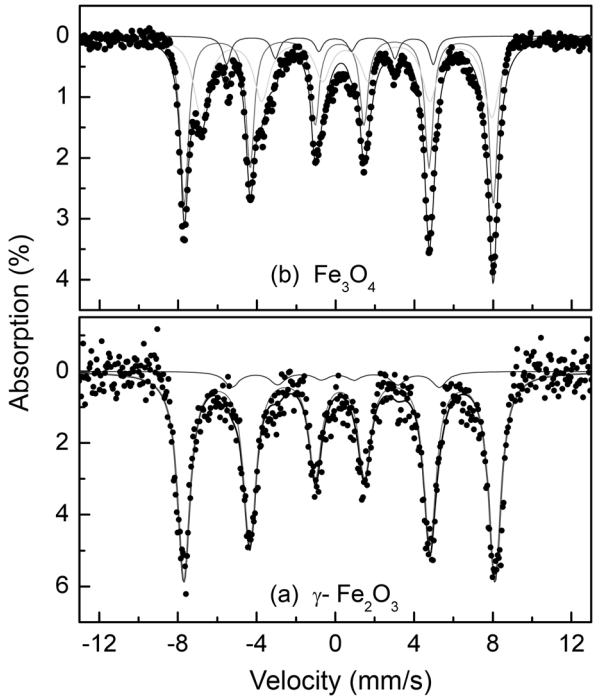

Fig. 5. Mössbauer spectra for (a) γ-Fe_2O_3 and α-Fe, and (b) Fe_3O_4 and α-Fe.

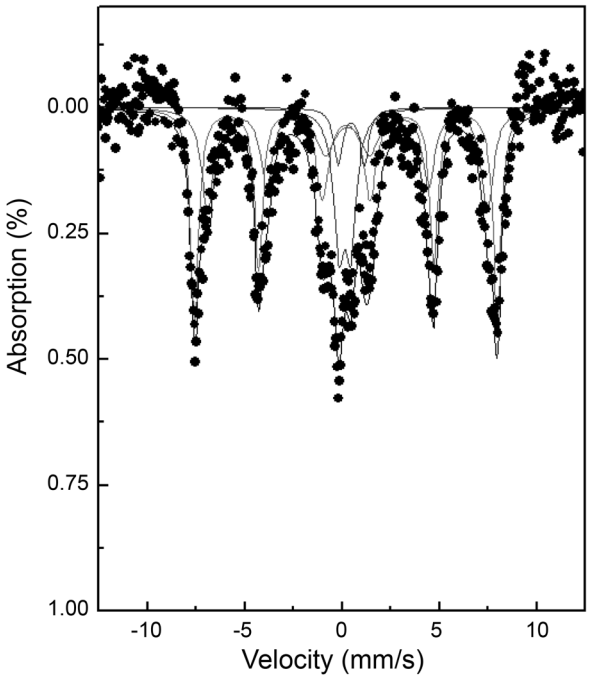

Fig. 6. Mössbauer spectrum for $NiFe_2O_4$ measured at 295 K.

and 93%, respectively. The Mössbauer spectrum indicated magnetic hyperfine fields due to particle sizes of 14 to 30 nm [13]. The Mössbauer spectrum at room temperature in Fig. 5(b) consists of 3 sets of sextet Lorentzian lines. Three superimposed sextets corresponded to α-Fe, Fe^{2+}, and Fe^{3+} of Fe_3O_4, respectively [13]. The fraction of spectrum absorption indicated that most particles became magnetically ordered. A detailed analysis yielded respective amounts of α-Fe and Fe_3O_4 at 8 and 92%.

Characterization of the crystal structure of the powders was carried out by x-ray diffraction (XRD). The positions and relative intensities of all the main diffraction patterns and characteristic reflections, such as (220), (311), (222), (400), (422), (511), and (440), as well as the calculated lattice parameters, were in agreement with those in the standard XRD card (JCPDS10-325) of Ni-ferrite. The peak arising from (400), located near 2° of 43°, was too large. This peak position was very close to the main peak of NiO. With the observation of each peak, it was clarified that a small amount of NiO was contained in the ferrite. The estimated amount of NiO was 7% by comparing with peak intensities, resulting from different vapour cooling temperatures between Ni and Fe. The range of particle size was 8 to 22 nm, comparable to the crystallite size calculated from the XRD. A specific surface area of 8.5 m^2/g measured by BET contributed to an estimated average particle size of 13 nm. In the lattice of the spinel compound, there were 2 kinds of oxygen polyhedra, octahedron (O_h) and tetrahedron (T_d). In the lattice of the nickel ferrite, with a completely inverse spinel structure, there were an equal number of Fe^{3+} ions at the T_d and O_h sites, respectively [3]. However, as Fig. 6 shows, there were 2 sets of sextet Lorentzian and 2 sets of doublets in the Mössbauer spectrum for Ni-ferrite. The 2 sets of sextets correspond to trivalent iron ranging from 12 to 25 nm at the T_d and the O_h sites. One doublet corresponds to a trivalent iron ranging at and below 12 nm, while the other indicates the existence of the Fe^{2+} ion ranging at and below 12 nm at the O_h site. A detailed analysis yielded 9 and 7% for the Fe^{3+} and Fe^{2+} at the octahedral site, respectively. The isomer shift of 0.54 (mm/s) in the second doublet indicates that the sample contains Fe^{2+} in the ionic state. The presence of Fe^{2+} is predominantly due to the hopping of electrons from Fe^{3+} to Fe^{2+}, as follows:

$$Fe^{3+} \Leftrightarrow Fe^{2+}, Fe^{3+}$$

From the results of the Mössbauer spectrum, Ni-ferrite synthesized by LGC includes an unusual ionic state [3]. The presence of Fe^{2+} is justified by cation vacancies in the ferrite lattice and the possibility of the presence of both Ni^{3+} ions and oxygen vacancies could be considered for the charge compensation in the ferrite. It is looked forwarded that the as prepared sample shows the high catalytic effect due to the oxygen vacancy on the surface layer, when it is used as catalyst in the chemical reaction [16].

4. Conclusions

Nanocrystalline Ni and ferrite (Fe_3O_4 and $NiFe_2O_4$) were synthesized by a levitational gas condensation (LGC) method using wire feeding (WF) and micron powder feeding (MPF) systems. The magnetic properties were characterized using vibrating sample magnetometry (VSM) and Mössbauer spectroscopy. The Mössbauer spectra revealed the presence of a superparamagnetic phase with ionic states of Fe^{2+} and Fe^{3+}, such that the spinel-type structures of Fe_3O_4 and γ-Fe_2O_3 could be distinguished by Mössbauer spectroscopy. The size and shape of the nanopowders were investigated by transmission microscopy (TEM). The surface effect might influence the magnetic hysteresis behavior of the nanopowders. In the case of Ni-ferrite, it consisted of single domain particles that included an unusual ionic state. The presented, simple and environmental friendly synthesis using metal powders as parent materials can be extended to prepare other nanoparticles with scientifically interesting properties.

Acknowledgment

This work was supported by Cooperation Research Project funded by Ministry of Education, Science and Technology, Republic of Korea.

References

[1] H. Morrish and K. Haneda, J. Appl. Phys. **52**, 2496 (1981).
[2] J. Fang, N. Shama, L. D. Tung, E. Y. Shin, and A. J. O'Connor, J. Appl. Phys. **93**, 7483 (2003).
[3] Y. Kinemuchi, K. Ishizaka, H. Suematsu, W. Jiang, and K. Yasui, Thin Solid Film **407**, 109 (2002).
[4] K. V. P. M. Shafi, Y. Koltypin, and A. Gedanken, J. Phys. Chem. B **101**, 6409 (1997).
[5] Y. Shi, J. Ding, and X. Liu, J. Magn. Magm. Mater. **205**, 249 (1999).
[6] Y. R. Uhm, W. W. Kim, and C. K. Rhee, Phys. Stat. Sol. A **201**, 1934 (2004).
[7] Y. R. Uhm, J. H. Park, W. W. Kim, C.-H. Cho, and C. K. Rhee, Mater, Sci. Eng. B **106**, 224 (2004).
[8] Y. R. Uhm, W. W. Kim, C. K. Rhee, S. J. Kim, and C. S. Kim, J. Appl. Phys. **93**, 7196 (2003).
[9] Y. R. Uhm, B. S. Han, M. K. Lee, S. J. Hong, and C. K. Rhee, Mater, Sci. Eng. A **449-451**, 813 (2007).
[10] Y. R. Uhm and C. S. Kim, J. Appl. Phys. **89**, 7344 (2001).
[11] B. D. Cullity, Introduction to Magnetic Materials (Addison-Wesley, Reading, MA, 1972).
[12] A. Ye, Yermakov, M. A. Uimin, A. A. Mysik, A. Yu, korobeinikov, A. V. Korolyov, N. V. Mushnikov, T. Goto, V. S. Gavoko, and N. N. Schegoleva, Mater. Sci. Forum, **386-388**, 455 (2002).
[13] X. N. Xu, Y. Wolfus, A. Shaulov, Y. Yeshurun, I. Felner, I. Nowik, Yu. Koltypin, and A. Gedanken, J. Appl. Phys. **91**, 4611 (2002).
[14] A. A. Novakova, V. Yu. Lanchinskaya, A. V. Volkov, T. S. Gendler, T. Yu. Kiseleva, M. A. Moskvina, and S. B. Zezin, J. Magn. Magn. Mater. **258-259**, 354 (2003).
[15] R. M. Cornell and U. Schwertmann, The Iron Oxides, (Wiley-VCH, Weinheim, 1996).
[16] H. Falcón, R. E. Carbonio, and J. L. G. Fierro, J. Catal. **203**, 264 (2001).